Proceedings of ISFOG 2025
5TH INTERNATIONAL SYMPOSIUM ON
FRONTIERS IN OFFSHORE GEOTECHNICS
Nantes, France | June 9-13 2025

ISBN 978-2-85782-758-0

Numerical Analysis on the Impingement Pressure and Excavation of Clay by Mass Flow Jet Trenching Considering the Nozzle Moving Speed

Long Yu[1*]
Dalian University of Technology, Dalian, Liaoning Province, China
Zeren Fan[1], Yunrui Han[1] and Guixi Jiang[1]
Dalian University of Technology, Dalian, Liaoning Province, China
**longyu@dlut.edu.cn*

ABSTRACT: In ocean engineering, jet trencher is often used to bury the pipelines and cables in seabed. The excavation of sediment by a water jet is a complex process, and the introduction of a moving jet further intensifies this complexity. This study aims to investigate the effect of nozzle travel speed by carrying out a series of numerical analyses. The CFD method (Computational fluid dynamics) is employed to simulate the moving impinging jet and excavation. The numerical results of impinging pressure and trench depth show good agreement with previous experimental results. As the nozzle moving speed increases, the peak impinging pressure initially remains constant and then decreases linearly. A novel trenching break threshold prediction procedure is proposed and validated. Finally, a trenching depth prediction model is proposed, which takes into account both jet parameters and clay strength parameters.

Keywords: Trenching, CFD, cohesive soil, impinging pressure

1 INTRODUCTION

In the exploitation of marine energy and resources, pipelines and cables play an important role in transporting information and resources. To prevent the risk of hostile seabed intervention from fishing, anchoring and other accidents, pipelines and cables can be buried beneath seabed (Gooding et al., 2012; Njock et al., 2020). Similar to dredging engineering, the jet trencher can penetrate in the seabed and form a trench with high velocity water jet, as shown in Figure. 1.

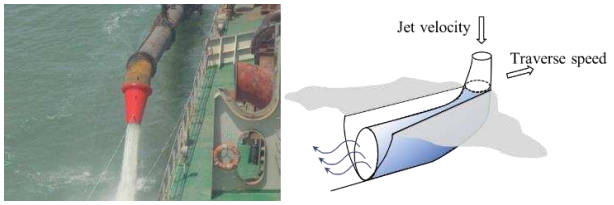

Figure 1. Trenching operation of jet trencher (Nobel, 2013)

A number of experimental and numerical studies have been performed on the fixed jet excavation problem. Studies by Wang et al. (2017) and Chen et al. (2023) examined the flow field and impinging pressure of a submerged water impinging jet using particle image velocimetry (PIV) and pressure measurements, highlighting the characteristics of velocity field and pressure distribution around the impingement region. Liu et al. (2023) simulated double-row jet on rigid plate and conducted experimental tests of fixed jet excavation of cohesive soil. They presented a relationship between impinging pressure and crater depth. Several researchers suggested that for cohesive sediment, failure occurs only when impinging pressure exceeds the bearing capacity of soil, which is related to undrained shear strength, s_u, and this principle also applies to moving jet excavation (Nobel, 2013; Qiu et al., 2024).

For moving jet excavation, the trench size does not only relate to the jet velocity v_j and impinging height H, but also to the nozzle moving speed v_t. Yeh et al. (2009) studied the influence of nozzle moving speed through a series of large-scale experimental tests, and found that the faster nozzle movement speed gave the shallower trench depth. Nobel (2013) conducted a series of physical experiments to study the relationship between jet dynamic pressure, soil strength, and trench depth. Based on Nobel's work, Wang et al. (2021) established a two-phase CFD model to explore the soil failure mechanism of moving jet trenching. However, limited research has

been conducted to investigate the quantitative effects of the nozzle moving speed on excavation.

The present work simulates the process of moving impinging jet on rigid ground and moving jet excavation of clay with the two-phase CFD model. The effect of nozzle moving speed on the impinging pressure are presented. A method to predict whether a jet can break the seabed are developed, by linking the jet parameters and soil strength parameters. A trenching depth prediction model are also proposed.

2 MODELS AND VERIFICATIONS

The ANSYS CFX 2022R1, a general purpose computational fluid dynamics (CFD) software including a solver based on the finite volume method (FVM), has been adopted in this study. The moving impinging jet on a rigid plate was simulated by the single phase fluid model to reveal the relationship between impinging characteristics and nozzle moving speed. The nozzle diameter d is 0.4m; the impinging height is H=8d, and the jet velocity v_j is 8 m/s. The nozzle moving speed v_t varies from 0 to 1 m/s, in which v_t = 0 m/s means the fixed impinging jet. The side and top surface of the domain are set as opening boundaries, and bottom surface are set as non-slip wall.

The model of jet on a rigid plate is verified by comparing with the experiments in Wang et al. (2017). Figure. 2 shows the comparison of pressure coefficient:

$$C_p = \frac{p}{\frac{1}{2}\rho_w v_j^2} \qquad (1)$$

where p (Pa) is the impinging pressure on the bottom surface, ρ_w (kg/m^3) is the density of water. It can be seen that the present results agree well the the experiments.

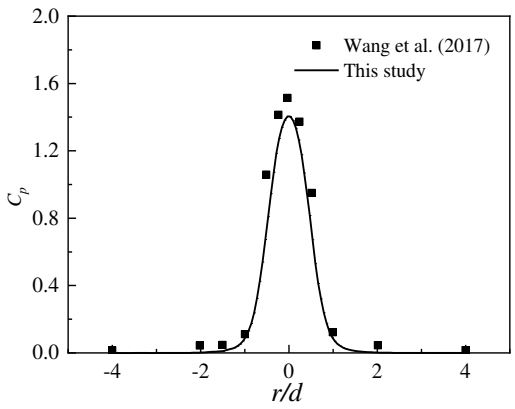

Figure 2. Impinging pressure distribution comparing with experimental results

The moving jet excavation of clay was simulated by the two-phase fluid model, in which the cohesive soil is modelled as a non-Newtonian fluid, as shown in Figure 3. This method has been successfully used for capturing the interaction and mechanisms of structure-sediment. (Dutta and Hawlader, 2019).

In the two-phase fluid model, a common flow field is shared by water and clay, as well as other relevant fields such as pressure and turbulence. The k-w SST turbulence model is adopted to capture the behavior of high velocity jet.

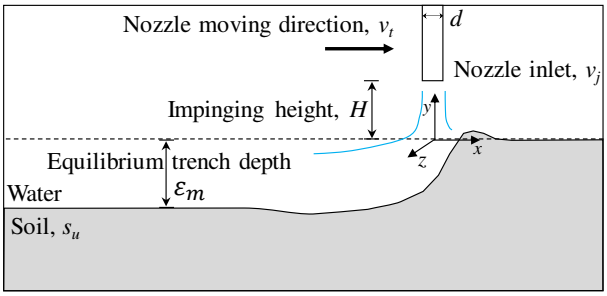

Figure 3. Schematic of moving jet erosion. Changing the bottom soil to a rigid wall is called moving impinging jet

The fluid shear strength is defined as:

$$\tau = \mu\dot{\gamma} \qquad (2)$$

where μ (Pa·s) is the dynamic viscosity, which can be expressed for non-Newtonian fluid as:

$$\mu = \frac{\tau_0}{\dot{\gamma}} + \mu_p = \frac{s_u}{\dot{\gamma}} \qquad (3)$$

where τ_0 (Pa) is the yield stress, which can be represented by the undrained shear strength of clay, s_u (Pa); μ_p (Pa·s) is the plastic viscosity and set to zero here; $\dot{\gamma}$ (s^{-1}) represents the second invariant of the strain-rate tensor.

As the nozzle moves forward, the mesh around nozzle may be distorted dramatically. In this study, a remeshing method has been adopted to solve this problem. Therefore, once the grid distortion reaches a certain threshold, CFX will halt the computation. Subsequently, a new set of grids will be regenerated using the meshing software MESHING within ANSYS. CFX will then read the newly generated grids, automatically configure the pre - processing parameters, and resume the solution process. This approach realizes the continuous forward movement of the nozzle. (Huang et al., 2019). The Dynamic grid (the mesh boundary can move during transient simulation) and grid remesh technology enable maintenance of high computational accuracy for moving jet.

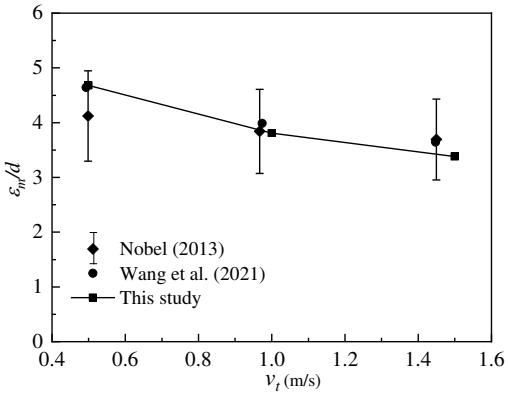

Figure 4. Verification of normalized trench depth for moving jet trenching, the uncertainty of Nobel's experimental work is 20%

Identical to Nobel (2013) and Wang et al. (2021), a submerged water jet trenching process has been simulated, in which the impinging height is H/d=2/3, jet ratio P_j/s_u=19.5. Jet pressure P_j is defined as: $P_j = 0.5\rho_w v_j^2$. The normalized trench depth from the present numerical simulations falls within the range of the experimental results, as shown in Figure 4. It can be seen that as nozzle moving speed v_t increases the trench depth decreases, this is because increasing v_t may reduce the impinging pressure. The relationship between impinging pressure and v_t will be discussed later.

3 RESULTS AND DISCUSSION

3.1 Jet impinging pressure on rigid plate

The underwater jet on a rigid plate was simulated to study the impinging pressure. The fluid velocity field for fixed jet and moving jet are shown in Figure 5 (a, b). For the fixed impinging jet, the velocity is symmetric about the central axis of the nozzle. The potential core is almost a triangle. With the development of jet, the jet column gets wider, because the jet entrains the surrounding static water. The overall flow field agrees well with Rajaratnam (1976). Figure 5(b) shows the case of nozzle speed of v_t=0.8 m/s. The potential core deviated backwards because of the drag resistance of surrounding water. As the jet developing from the nozzle to the bottom plate, the entrainment effect becomes more pronounced, and the jet velocity gradually decreases, making it difficult to maintain vertical development. In the free jet region, due to the movement of the nozzle, the pressure behind the jet drops below that of the ambient water. As a result, the entrainment phenomenon in this area becomes more pronounced. In the impingement region, it can be seen that the stagnation point (SP) deflected backward.

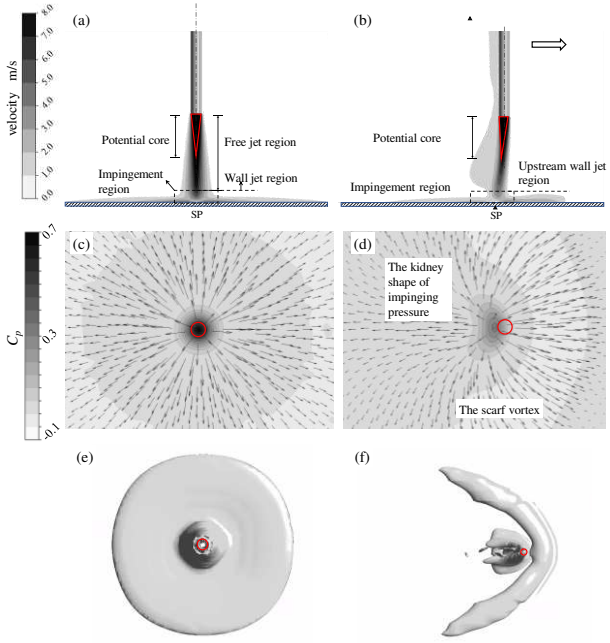

Figure 5. Comparison of velocity contour and pressure contour, and vorticity for fixed impinging jet and moving impinging jet (v_t=0.8 m/s) (the red triangle represents the potential core, and the red circle is nozzle, and the velocity vector is shown in (c) and (d), (e) and (f) are the isosurface of Q-criterion, Q=0.03 s^{-2})

In the wall jet region, the upstream wall jet is moving forward and interacting with the surrounding water, forming a vortex and wrapping around the impinging jet like a scarf. The low-pressure region in Figure 5d is the scarf vortex. This phenomenon is similar with the impinging jet in crossflow (Barata, 1996).

Figure 5 (c,d) shows the pressure distribution and the flow horizontal velocity on the rigid bottom plate of fixed and moving impinging jets. It can also be seen that the stagnation point of the moving jet deflected backward. The pressure distribution of the moving jet tends to be like a kidney shape (the deep color erea in Fig. 5(d)). Figure 5 (e, f) show the top view of vorticity contour, where the scarf vortex is prominent.

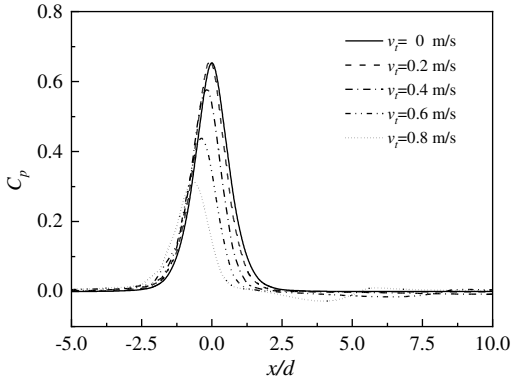

Figure 6. Normalized impinging pressure distribution for v_t=0 to 0.8 m/s

Figure 6 shows the pressure distribution on the rigid bottom along the nozzle moving direction. It can be obviously seen that the increase in v_t reduces the impinging pressure. The reduction is limited when $v_t \leqslant 0.2$ m/s. With further increase in v_t, both the peak impinging pressure and the spreading range reduces obviously. As v_t increases to 0.8 m/s, the maximum impinging pressure value decreases to 47% than $v_t = 0$.

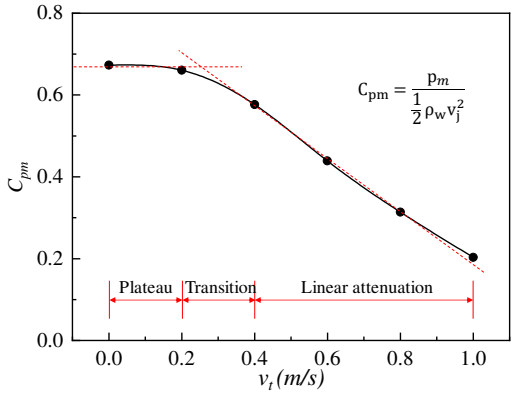

Figure 7. Variation of maximum pressure coefficient to nozzle moving speed

The relationship of the maximum impinging pressure coefficient C_{pm} with the nozzle moving speed is shown in Figure 7. As v_t < 0.2 m/s, the maximum impinging pressure changes very little. For v_t > 0.4 m/s, C_{pm} decreases almost linearly with the increase of v_t. This chart quantifies the effect of nozzle moving speed on impinging pressure, in other words, on trenching ability. It should be noted that this curve is from the case of H = 8 m, v_j = 8 m/s, d = 0.4m. More cases will be studied in the near future.

3.2 Determination of the jet condition to form trench

For the trenching problem, it is crucial to determine the required jet condition to overcome the seabed ultimate resistance to achieve the required depth below mudline. The 'active' factors may include the jet velocity, impinging height, nozzle moving speed, etc., while the 'resistance' factor is mainly the soil strength. This section attempts to find the threshold state for a jet problem that the jet is 'strong' enough to break the seabed. Wang and Song (2019) examined the fixed jet excavation on clay with CFD method, highlighting the equilibrium state is related to the impinging pressure and soil strength. Experiments results (Machin and Allan (2011)) on cohesive soil also indicates that the initial penetration is an almost instantaneous undrained shear failure, with the threshold trenching breaking state can be interpreted by soil bearing capacity theory:

$$p > q = N_c \cdot s_u \qquad (4)$$

here, s_u (Pa) is the undrained shear strength of cohesive soil, and N_c is the bearing capacity factor (N_c=6 recommend by Machin and Allan (2011)), q (Pa) is the bearing capacity of soil. As the impinging pressure p exceeds q, the seabed can be broken thus the trenching works.

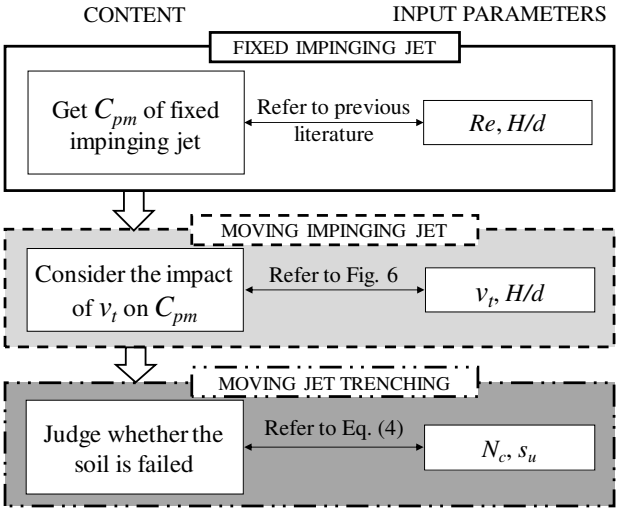

Figure 8. Flowchart of trenching breaking state determination

For submerged circular moving jet vertical to cohesive soil, Figure 8 shows a flowchart for determining whether the soil is in failure.

Firstly, the maximum fixed impinging pressure value can be calculated according to the jet parameters, jet velocity v_j and impinging height H. Secondly, the influence of nozzle moving speed v_t on maximum impinging pressure can be obtained from Figure 7. Finally, formula (4) can be used to determine whether the jet can break the soil.

3.3 Moving jet trenching on cohesive soil

In this section, the trenching process of different jet parameters and soil undrained shear strength are studied. Some cases are conducted for v_j = 2~16m/s, H/d = 2~12, and s_u = 1~8 kPa, , and the soil density is set to 1600 kg/m^3.

Figure. 9 shows the trench profiles of different soil strength, the smaller the soil strength, the deeper trench depth.

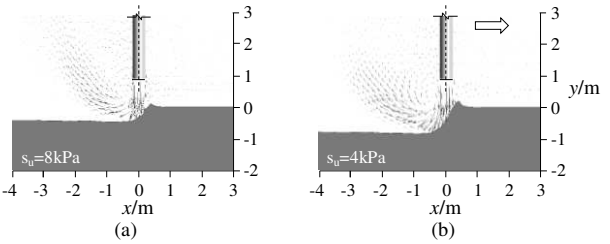

Figure 9. trench profile for different soil undrained shear strength

The trench depth pridiction model is shown in Figure 10. The normalized trenching parameter, T_r is proposed:

$$T_r = 2\frac{P_j}{s_u}\left(\frac{d}{H+d}\right)^2 \cdot \left(\frac{v_j}{v_t}\right)^{\frac{1}{2}} \quad (5)$$

where P_j/s_u means the jet ratio, which is proposed in Nobel (2013), and represent the ratio of jet force to soil resistance, $\frac{d}{H+d}$ and $\frac{v_j}{v_t}$ represent the influence of impinging height and nozzle moving speed. Increasing impinging pressure or jet velocity, or decreasing soil strength, impinging height, or nozzle moving speed results in higher T_r and thus deeper trench depth. The predicted results agree well with the reported experimental data.

$$\frac{\varepsilon_m}{d} = 0.78 \cdot T_r^{0.45} \quad (6)$$

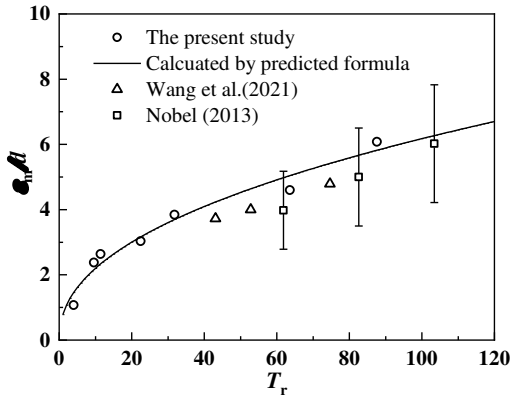

Figure 10. comparison of predicted results and experimental data

3.4 Validation of threshold trenching state

To validate the proposed workflow presented in Figure 8, numerical simulations of jet trenching on cohesive soil were performed and analysed.

Table 1. Characteristics of jet trenching cases

v_j (m/s)	H/d	v_t (m/s)	p_m (Pa)	q_c (Pa)
8	8	0.2	21142	21000
		0.4	18447	
		0.6	14039	
		0.8	10045	

The jet parameters and impinging pressure and the bearing capacity of soil are shown in Table 1, p_m represents the maximum impinging pressure. The soil undrained strength is set to 3.5kPa, and corresponding to critical bearing capacity q_c is 21000 Pa.

Figure 11 shows the trench profile for different v_t, it can be seen that as $v_t \geq 0.4$ m/s, the impinging pressure is too weak to make trench, as $v_t \leq 0.2$ m/s, the impinging pressure reach the trenching threshold, and a shallow trench of 1d depth is formed (Nobel, 2013).

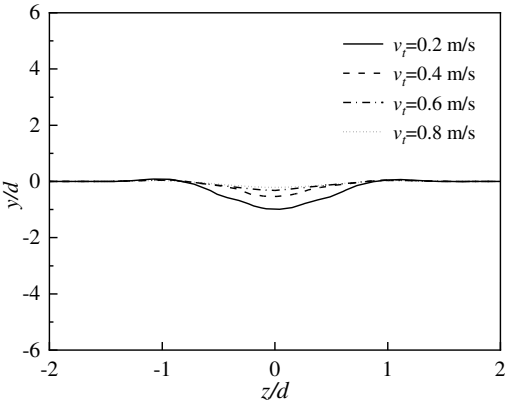

Figure 11. Trench profile of different nozzle moving speed

4 CONCLUSIONS

This study aims to analyse the effect of nozzle moving speed on the jet trenching process on cohesive seabed. The impinging pressure distribution and trenching capacity have been validated by comparing with existing references. In fact, the influence of nozzle moving speed on jet trenching is primarily embodied in the attenuation effect on the impinging pressure, that is, the greater the moving speed, the smaller the jet impinging pressure. The following conclusions can be summarized:

(1) A series of CFD models have been conducted to investigate the discrepancies in the

impinging pressure field of fixed jet and moving jet. For fixed impinging jet, the flow field and impinging pressure field are axisymmetric, however, for moving impinging jet, the trailing edge of potential core and stagnation point are deflected backward and the impinging pressure shape is compressed due to the resistance of surrounding static water.

(2) Based on the relationship between impinging pressure and nozzle moving speed, a flowchart of trenching breaking state determination has been proposed. Utilizing basic jet and soil parameters—v_j, H, v_t, and s_u—the procedure can determine whether soil can be break under these conditions. The results demonstrate an encouraging trend, indicating that the prediction procedure may be helpful for engineering practice.

(3) A prediction formula for the trenching depth has been proposed which considering jet ratio, impinging height and nozzle moving speed. The comparison with previous studies shows a good agreement. More parameter analysis is intended to be conducted in the future.

AUTHOR CONTRIBUTION STATEMENT

Long Yu: Funding acquisition, Supervision, Conceptualization, Project administration. **Zeren Fan**: Conceptualization, Methodology, Validation, Writing & editing. **Yunrui Han**: original draft, Writing – review. **Guixi Jiang**: Reviewing and Editing, Supervision.

ACKNOWLEDGEMENTS

The authors are grateful for the financial support provided by the National Natural Science Foundation of China (Grant nos. 52331010, 52171252 , 52231011, and 52109115), and the Fundamental Research Funds for the Central Universities (DUT22QN236).

REFERENCE

Barata, J.M., 1996. Fountain flows produced by multiple impinging jets in a crossflow. *AIAA J.* 34 (12), 2523-2530.

Chen, J., Wang, X., Shi, H., Si, J.-H., 2023. Experimental investigation on flow characteristics of vertical and oblique circular impinging jet. *Phys. Fluids* 35 (5).

Dutta, S., Hawlader, B., 2019. Pipeline-soil-water interaction modelling for submarine landslide impact on suspended offshore pipelines. *Geotechnique* 69 (1), 29-41.

Gooding, S., Black, K., Boyde, P., Boyes, S., 2012. Environmental impact of subsea trenching operations. *SUT Offshore Site Investigation and Geotechnics*, SUT-OSIG-12-20.

Huang, Z., Xiong, Y., Xu, Y., 2019. The simulation of deformation and vibration characteristics of a flexible hydrofoil based on static and transient FSI. *Ocean Eng* 182, 61-74.

Liu, X., Chen, X., Wei, J., Jin, S., Gao, X., Sun, G., Yan, J., Lu, Q., 2023. Study on sediment erosion generated by a deep-sea polymetallic-nodule collector based on double-row jet. *Ocean Eng* 285, 115220.

Machin, J., Allan, P., 2011. State-of-the-art jet trenching analysis in stiff clays, *Frontiers in Offshore Geotechnics II, Proceedings of the 2nd International Symposium on Frontiers in Offshore Geotechnics*, pp. 871-876.

Njock, P.G.A., Zheng, Q., Zhang, N., Xu, Y.S., 2020. Perspective Review on Subsea Jet Trenching Technology and Modeling. *Journal of Marine Science and Engineering* 8 (6), 27.

Nobel, A.J., 2013. *On the excavation process of a moving vertical jet in cohesive soil*, Delft: TU Delft.

Qiu, Y.Q., Lan, X.D., Yang, Z.P., Wang, G.S., Liu, J., 2024. Study on the mechanism of soil erosion by submerged water jet vertical scouring in cohesive soils. *Ocean Eng* 311, 11.

Rajaratnam, N., 1976. Turbulent jets. Elsevier.

Wang, B.Y., van Rhee, C., Nobel, A., Keetels, G., 2021. Modeling the hydraulic excavation of cohesive soil by a moving vertical jet. *Ocean Eng* 227, 13.

Wang, C., Wang, X.K., Shi, W.D., Lu, W.G., Tan, S.K., Zhou, L., 2017. Experimental investigation on impingement of a submerged circular water jet at varying impinging angles and Reynolds numbers. *Exp. Therm. Fluid Sci*. 89, 189-198.

Wang, T., Song, B., 2019. Study on deepwater conductor jet excavation mechanism in cohesive soil. *Appl Ocean Res* 82, 225-235.

Yeh, P.H., Chang, K.A., Henriksen, J., Edge, B., Chang, P., Silver, A., Vargas, A., 2009. Large-scale laboratory experiment on erosion of sand beds by moving circular vertical jets. *Ocean Eng* 36 (3-4), 248-255.